Pages: 58-69 / Vol.18 / Issue 1 / Winter - Spring 2025

**Journal of Aerospace Science and Technology**

Journal Homepage: www.jast.ias.ir

**Original Research Article**

# Experimental Study on the Performance of a Symmetrical Twin Air Intake System

**Asghar Fazli[1], Afshin Abdi[2] , and Mostafa Mahmoodi[3*]**

1. Air Research Center, Air Industry Org, Iran
2. Faculty of Aerospace Engineering, Amirkabir University of Technology, Iran
3. Faculty of Aerospace Engineering, Malek Ashtar University of Technology, Tehran, Iran

**ARTICLE INFO**

**Received:** 10 June 2024
**Revised:** 07 March 2025
**Accepted:** 09 March 2025
**Available online:** 12 April 2025

**KEYWORDS:**

Air-intake
Experimental
Total Pressure,
Recovery
Duct performance
Twin air-intake

DOI:
https://doi.org/10.22034/jast.2025.462215.1192

**ABSTRACT**

*The main purpose of an air inlet is to supply air to the engine in a steady and efficient manner while achieving the maximum total pressure recovery. A twin air intake consists of two S-ducts that join at the downstream end to supply air to a single engine. In the present study, a Y-duct inlet with vertical and horizontal offsets and a part of the aircraft fuselage affecting the duct performance were modeled. Its performance was tested experimentally by measuring total pressure recovery, flow distortion, and static pressure on the duct walls for different sideslip angles and angles of attack. The aircraft wing had a leading edge extension (LEX), which projected over the inlet cowl and impacted the inlet's performance. The tests were performed in a subsonic, open-circuit wind tunnel. In all tests, the Mach number was kept at 0.15. Based on the results, the flow distortion coefficient at the exit plane of the duct was found to be 29.2%, and the maximum total pressure loss was 1.75%.*

## 1. INTRODUCTION

The air inlet is a device that is designed to direct the free stream airflow towards the intake plane of the engine under the right conditions. It is also used to transform the free stream kinetic energy into static pressure at the compressor inlet plane [1]. It can be seen that as the flight Mach number increases, the inlet design becomes more complicated and sensitive. The performance of the inlet is a critical factor in determining the efficiency of the engine and the net thrust; the maximum thrust is obtained when the inlet can provide the necessary airflow at the highest total pressure to the compressor face [2-3]. There are many pieces of research dedicated to different types of air inlets: experimental [4] and numerical research of the flow through S-ducts, the simulation of the secondary and separated flows in S-ducts [5], the flow optimization in S-ducts [6-7-8-9-10-11-12]. A twin-duct inlet is a specialized configuration employed in single-engine aircraft. Twin air intake is the prime segment of a single-

* Corresponding Author's Email: mostafamahmoodi@mut.ac.ir

engine aircraft, which is employed to deliver ambient air to the engine [13].In such twin air intakes, air is delivered into their two lone S-shaped limbs, which have centerline curvature and increasing cross-sectional area along the direction of the flow. These limbs merge into a single limb of duct leading to the engine [14]. In general, flow instability and asymmetry are inherent in twin-duct inlets, and in the worst-case scenarios, they can compromise the stability of an aircraft [15]. In addition, secondary vortices occur at the junction where the two duct branches join, leading to flow non-uniformity [16]. Martin and Holzhauser experimentally investigated the parameters affecting the flow stability characteristics in the inlet of a symmetrical twin air duct and showed that the flow instability and flow reversal are functions of the static pressure and recovery characteristics at the junction of the two ducts [17]. Sudhakar et al. investigated the "Jump phenomena" in Y-shaped intake ducts [18]. Patel et al. have numerically analyzed the performance of a rectangular Y-duct with a circular exit for different inlet flow conditions. They noted that a very large velocity gradient also led to increased flow distortion and decreased total pressure recovery at the duct outlet [19]. Saha also investigated twin-duct inlets with different inlet shapes and concluded that the inverse semi-elliptical inlet shape provided the best performance while the square duct inlet provided the worst performance [20]. Paul et al. proposed and experimentally investigated the active and passive flow control in twin-duct inlets [21]. Singh et al. studied the impact of corner rounding on the Y-duct inlet and found that the flow characteristics and inlet performance were enhanced up to a corner radius (r/D (h)) of 0.14 [22]. Seshadri et al. investigated the flow characteristics in a double-offset Y-shaped inlet [23]. Kotteda and Mittal studied the flow characteristics in a Y-inlet at supersonic speeds [24].

Additionally, several researchers in this field have worked on flow management and control in Y-shaped air inlets [25-26-27]. Owing to the unique shape of the Y-duct inlet, it typically features offsets in two planes. Based on the numerical investigations by Gopaliya and Chaudhary [28]. when a Y-shaped air inlet has both horizontal and vertical offsets, increasing the vertical offset decreases total pressure recovery and increases flow distortion.

In this research, the performance of a symmetrical Y-duct inlet was experimentally evaluated by analyzing total pressure recovery, flow distortion, and static pressure distribution on the duct walls for various angles of sideslip and angle of attack. The studied duct featured both vertical and horizontal offsets. A portion of the aircraft fuselage influencing the inlet was also constructed alongside the duct to account for the fuselage's effect on the duct's performance. The aircraft wing had a leading-edge extension (LEX), and the inlet cowl was situated in its shadow.

## 2. DUCT CONFIGURATION

The tested air inlet was a twin-duct comprising two S-ducts merged at the downstream end into a cylindrical section. The duct and a portion of the aircraft fuselage affecting the inlet flow quality were designed and constructed. The aircraft featured a LEX, and the inlet cowl was positioned in its shadow. The inlet lip cross-section was approximately rectangular, with stagger angles of 28.41° and 33.28° in the top and side views, respectively. Air intake and its geometric details are depicted in Fig. 1.

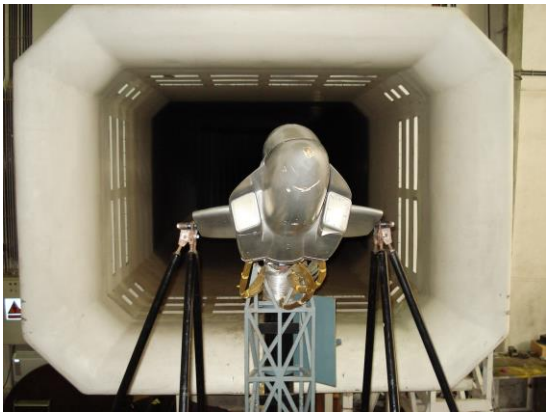

**Fig. 1**. Air intake with the aircraft fuselage in the wind tunnel.

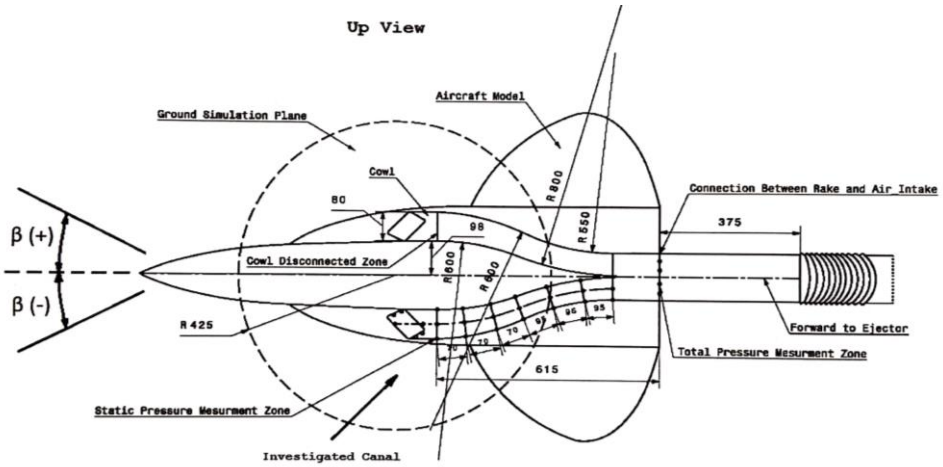


**Fig. 2**. Top view of the air inlet duct with associated components.

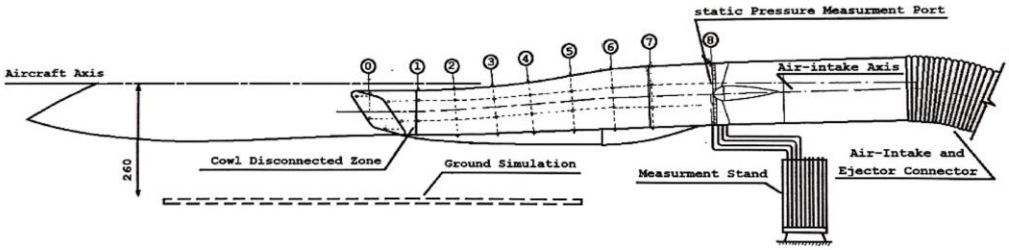


**Fig. 3** Side view of the air inlet duct with associated component.

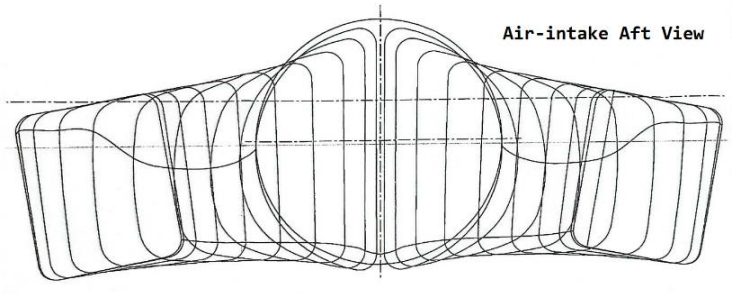


**Fig. 4** Schematic of the air inlet duct (Aft view).

## 3. EXPERIMENTAL METHODOLOGY

### 3.1. Experimental Setup and Measurement Technique

In this section, the laboratory equipment, the pressure measurement process, and the method of calculating the main parameters of the channel are presented.

#### 3.1.1 Laboratory Equipment

The equipment required and related to the inlet testing included two ground jet engines, hoses connecting the duct to the data acquisition system, a 32-tube manometer, a pressure sensor device, a duct holding fixture, and others. Static pressure was measured at 72 locations along the duct length. The installed ports on the duct were connected via appropriate hoses to a device equipped with 128 pressure sensors. The sensor data was transmitted to the data acquisition system during testing, where the pressure values were simultaneously recorded. This system could record 30,000 data points per second for each sensor and simultaneously log data from 132 channels. Pressure sensing at the inlet lips and duct exit was in the form of both total and static pressures, while along the duct length, only static pressures were measured. The pressure sensor device is shown in Fig. **5**.

**Fig. 5.** Pressure sensor device.

Two ground jet engines, with a maximum suction flow rate of 1600 g/s, were utilized to draw air through the inlet duct. Fig. **6** illustrates a schematic of the engines and the equipment used to connect the model to them.

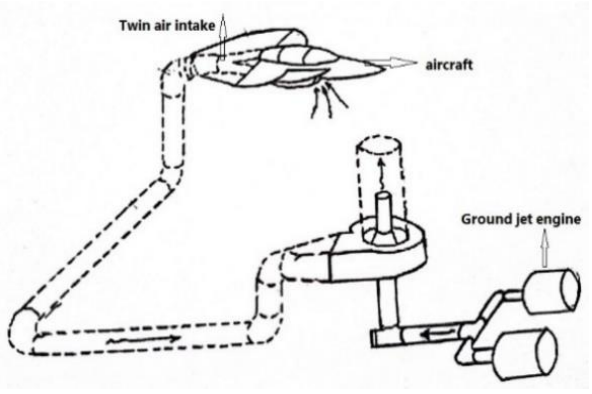


**Fig. 6.** Schematic of the engines and equipment for connecting the model.

The wind tunnel used for the tests was an open-circuit type with an open test section, as shown schematically in Fig. **7**.

The test section dimensions were 2.8 m (width) x 2.2 m (height), with a length of 4 m in the open configuration. The subsonic wind tunnel had a maximum flow speed of 50 m/s.

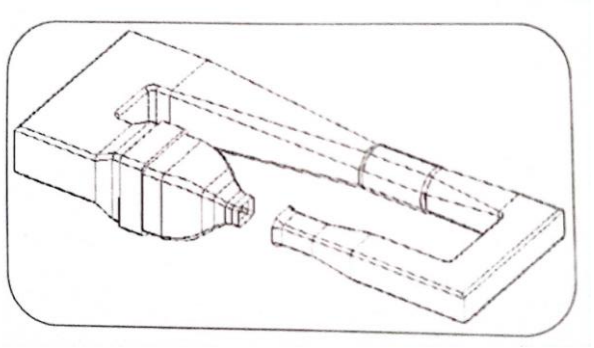

**Fig. 7**. Schematic of the wind tunnel used in the experiments.

### 3.1.2 Mass Flow Rate Measurement

The mass flow rate through the inlet duct must be measured as accurately as possible. In this regard, the desired level of accuracy is ±0.5%, which is quite challenging to attain. It is possible to achieve an accuracy of ±1%, and in cases where the flow is not uniform, errors of up to ±10% are possible. The data that is needed to calculate the duct mass flow rate is the static and total pressures at a point in the suction path. In the present study, the total and static pressures were measured at a section of the suction path in order to calculate the mass flow rate through the duct.

### 3.1.3 Total Pressure Measurement at the Duct Exit Plane

A rotating rake with 16 tubes for recording total pressures was used to measure the total pressure at the duct exit plane. The rake was designed to be installed at the duct exit, and by rotating and positioning it at different angles, the total pressure distribution across the exit plane was scanned. The exit plane was divided into 60° sectors, and during the experiments, pressures were recorded along the 60° radial lines. The employed rake, the position, number, and geometric dimensions of the installed tubes are shown in Fig. **8**.

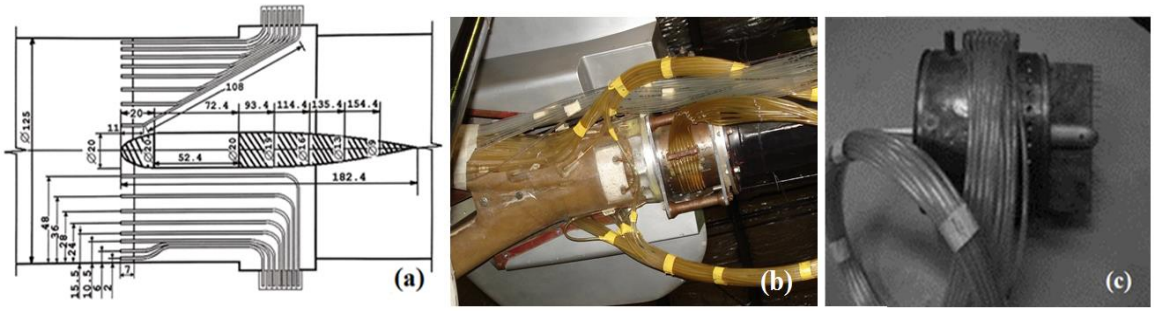


**Fig. 8.** Total pressure measurement rake at the duct exit: (a) Rake dimensions and positions of the total pressure measurement tubes on the rake, as well as (b) and (c) rake views.

### 3.1.4 Pressure Measurements at the Duct Inlet Plane

A suitable cowl was designed and constructed to measure the static and total pressures at the duct inlet plane, featuring 28 tubes for recording total pressure and 6 tubes for static pressure. The locations of the static and total pressure tubes are shown in Figure (8). This cowl could be attached or detached from the duct. Figure (8) depicts the constructed cowl in the installed and uninstalled states.

### 3.1.5. Pressure Measurements along the Duct Length

Only static pressures were measured along the duct length, utilizing 72 tubes. The locations and installation planes of the tubes at sections 1 to 8 of the studied duct are shown in Fig. **2** and Fig. **3**.

### 3.1.6. Test Procedure

First, the device was equipped with pressure sensors, and the data acquisition system was turned on. The data acquisition system was shifted, and the total and static pressure measurement hoses, which were mounted in a part of the suction path, were connected to the manometer. The engines were then started and brought to the required operating state. At this point, the data acquisition system captured the desired pressure values, as shown below. As the system captured 30,000 data points per second for each sensor, capturing the required values for 2 to 3 seconds was adequate for assessing the inlet performance. It should be noted that each specific test was recorded 3 to 4 times and compared. An average was taken from these multiple recordings for each specific test to minimize measurement errors. The data was initially captured in the form of voltages by the use of dedicated software and then calibrated to pressures using the specifications of the sensor

.

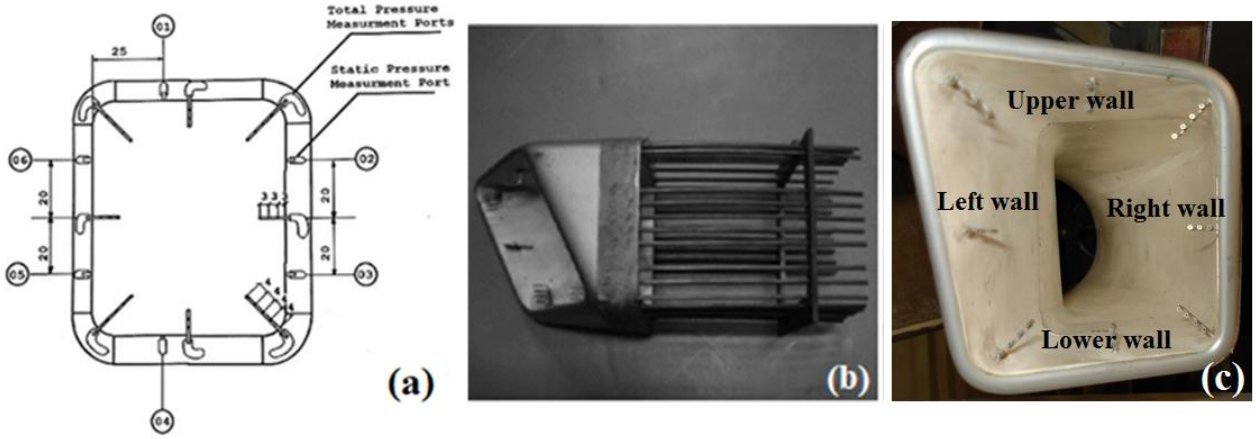


**Fig. 9.** Cowl for recording total and static pressures at the duct inlet: (a) Schematic of the locations of the total and static pressure tubes, (b) Side view of the cowl, (c) Front view of the cowl.

The given values were then checked using the manometer to ensure that they correspond with the manufacturer's recommendations. While plotting the graphs, it was realized that the data acquisition system captured and stored 30000 data points per second for each sensor, and thus, the data was massive. If an appropriate method of using this data were chosen, the accuracy of the results could be significantly improved. The averaging technique was used in this research.

### 3.2 Evaluation of Duct Performance

The duct's performance was evaluated by calculating the total pressure loss, static pressure coefficient on the duct walls, and distortion coefficient [29-31]:

### 3.2.1. Total Pressure Loss Calculation

The total pressure loss is obtained from Equation (2) [1]:

$$PR = \frac{P_{o,out}}{P_{\infty}} \qquad (1)$$

$$\Delta P = 1 - PR \qquad \text{.....} \qquad (2)$$

In Equation (1) [1], PR is the total pressure recovery, and $P_{o,out,}$ and $P_{\infty}$ are the total pressures at the channel outlet and free stream, respectively.

### 3.2.2. Flow Distortion Calculation

The flow distortion is defined by Equation (3) [1]:

$$DC_{60} = \frac{P_{60}}{q_f} \quad (3)$$

Where $q_f$ is the average dynamic head at the channel exit plane, and $P_{60}$ is calculated as follows [1]:

$$P_{60} = max\left(abs\left(P_a - P_f\right)\right) \quad (4)$$

Here, $P_f$ is the average total pressure at the channel exit plane, and $P_a$ is the average total pressure in an arbitrarily selected 60-degree sector of the duct exit plane.

### 3.2.3. Pressure coefficient (Cp) Calculation

The pressure coefficient (Cp) is a dimensionless number that describes the relative pressures throughout a flow field in fluid dynamics. It has been used in both aerodynamics and hydrodynamics to compare the pressure at a point in the flow field to the free stream static pressure. The pressure coefficient is defined as [32-33]:

$$C_P = \frac{P - P_\infty}{0.5\rho V_\infty^2} \quad (5)$$

Where:

(p) is the static pressure at the point of interest. ($P_\infty$) is the freestream static pressure (far from any disturbances).

(ρ) is the fluid density in the free stream. ($V_\infty$) is the freestream velocity of the fluid.

## 4. RESULTS AND DISCUSSION

In this section, the results obtained from the experiments are discussed.

### 4.1 Total Pressure Loss

To obtain the total pressure loss in the studied duct, experiments were conducted by varying the angle of attack from -10° to +40° and the sideslip angle at 0° and 15°, and the total pressure was recorded at the duct exit plane using the method described in Section 3.1.3. Subsequently, the duct pressure loss was determined using Equations 1 and 2. It should be noted that in all the conducted tests, the wind tunnel flow speed was v = 50 m/s, the ambient temperature was 300(k), and the ambient pressure was 87000 (kpa). The experimental results are presented in Fig. **10**. As the figure shows, increasing the angle of attack leads to an increase in the adverse pressure gradient on the duct's lower wall. This results in boundary layer thickening and, consequently, higher total pressure loss at the duct exit. The increase in total pressure loss occurs continuously with increasing angle of attack. However, a similar pattern occurs for negative angles of attack on the upper wall. Additionally, at a sideslip angle of 15°, the left duct wall is influenced by the fuselage shadow. In this case, the boundary layer formed on the aircraft fuselage surface is thicker than normal due to the sideslip angle, causing the fuselage boundary layer flow to enter the duct. In the conducted tests, there was no need to adjust the -15° sideslip angle to calculate the duct exit total pressure loss since the right duct simultaneously experiences the 15° sideslip angle corresponding to the left duct. As the two ducts merge at the exit, the effects of both positive and negative sideslip angles are simultaneously observed at the duct exit. A notable aspect of the present duct design is the stagger angle in the duct cowl (Fig. **9**) in the side and top views. Positive stagger could have a considerably favorable effect on the intake performance of incidence. Increasing the stagger angle decreases the maximum velocity on the inside of the lower lip and hence reduces the tendency to flow separation [1].

Meanwhile, the LEX structure improves the duct's performance at high AOA (by supporting the duct against the AOA of the inlet flow). The concept of sustaining intake performance at high angles of incidence by positioning an intake beneath the aircraft fuselage or LEX to both subsonic and supersonic aircraft and has been used many times in design. The principle is simply that when incidence is varied, the airflow direction at the intake is controlled by the aircraft surface, so to that extent the intake is 'not aware' of a change in attitude [1]. Hence, it degrades the duct's performance at AOA below zero. This is due to the fact that the LEX surface ingests low-energy boundary layer flow into the duct, and the boundary layer has been thickened by the adverse pressure gradient. Therefore, the pressure recovery parameter values for this duct are not equal when tested at an angle of attack of 10° and -10°.

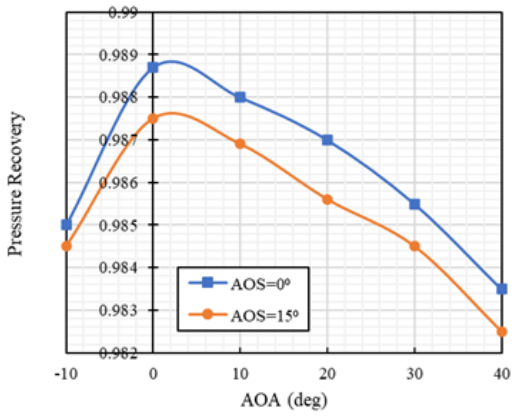


**Fig. 10.** Variation of the pressure recovery parameter with different angles of attack for sideslip angles of 0° and 15°.

### 4.2 Flow Distortion at the Duct Exit

To calculate the flow distortion at the duct exit, Equation 3 was employed. To determine $q_f$ in the experiments, Equation 4 was used. Specifically, the static and total pressures were recorded at a section along the suction path, and $q_f$ was calculated from their difference (considering the low Mach number flow, compressibility effects were neglected). Fig. **11** illustrates the 60° sector subdivision used in the present study.

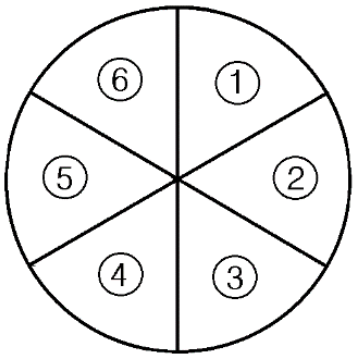


**Fig. 11.** Numbering scheme for the 60° sectors at the air inlet duct exit.

The calculations were done for angles of attack from -10° to 40° and sideslip angles of 0° and 15°. It can be seen that because of the merging of the two ducts at the exit, the flow distortion values will be the same for the 15° and 15° sideslip angles. As stated above, in all the tests, the wind tunnel speed was 50 m/s, the ambient temperature was 300(k), and the ambient pressure was 87000 (kpa). Fig. **12** illustrates the distribution of the flow distortion parameter at the duct exit plane for zero side slip angle and various angles of attack. As observed from the figure, at an angle of attack of -10°, the maximum flow distortion parameter is found to occur in sectors 1 and 6. In this regime, the presence of the LEX is seen to have a negative impact on the duct's performance because of the boundary layer growth on the LEX surface due to the adverse pressure gradient and the flow ingestion into the duct. It is also observed that as the angle of attack increases, the distortion values in these sectors become gradually smaller. Nevertheless, they are still above the average values of sectors 2 and 5 due to the vertical end walls of the two ducts and the losses that occur in these sectors. As the angle of attack is raised, the flow distortion in sectors 3 and 4, which are situated in the lower part of the duct, rises. It should be noted that there is no sharp rise in flow distortion beyond 10° due to the support provided by the LEX and the stagger angle in the duct cowl.

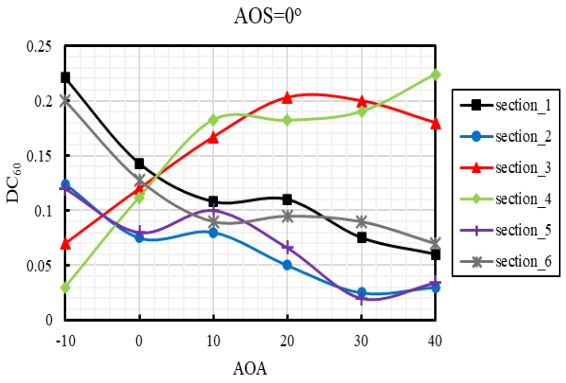


**Fig. 12.** Variation of the flow distortion parameter with angle of attack for different sectors at a zero sideslip angle.

Fig. **13** shows the variation of the flow distortion parameter with angle of attack for sideslip angles of 0° and 15°. Similar to the explanations provided in the previous section, at an angle of attack of -10°, the LEX has a detrimental effect on the duct's performance, which gradually diminishes as the angle of attack increases.

An increase in the flow distortion parameter with an increasing angle of attack is natural. The introduction of a sideslip angle causes asymmetry in the flow between the two ducts (the duct in the fuselage shadow experiences higher losses). This phenomenon leads to an increase in the flow distortion at all angles of attack when a sideslip angle is present. In this plot, for both sideslip angles of 0° and 15°, no significant increase is observed in the distortion parameter values with increasing angle of attack, which, as mentioned, is due to the presence of the LEX and the stagger angle in the inlet section.

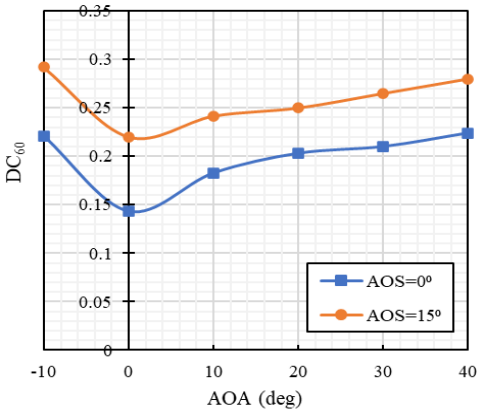


**Fig. 13.** Variation of the flow distortion parameter with angle of attack for sideslip angles of 0° and 15°.

### 4.3 Analysis of Static Pressure Coefficient Distribution on the Duct Walls

In this section, the distribution of the static pressure coefficient on the duct walls (top, bottom, left, and right, as shown in Fig. **9**(c)) is investigated under the influence of varying angles of attack and sideslip.

#### 4.3.1 Analysis of Static Pressure Coefficient Distribution on the Duct Walls for Different Angles of Attack

Fig. **14** illustrates the variation of the pressure coefficient along the duct walls with changes in the angle of attack.

Top Wall: Due to the supportive effect of the LEX, the flow enters the duct with minimal deflection. This small deflection translates to a minimal change in the pressure values on the surfaces compared to the free stream.

As the flow enters this section of the duct, the pressure coefficient is close to zero but negative

.

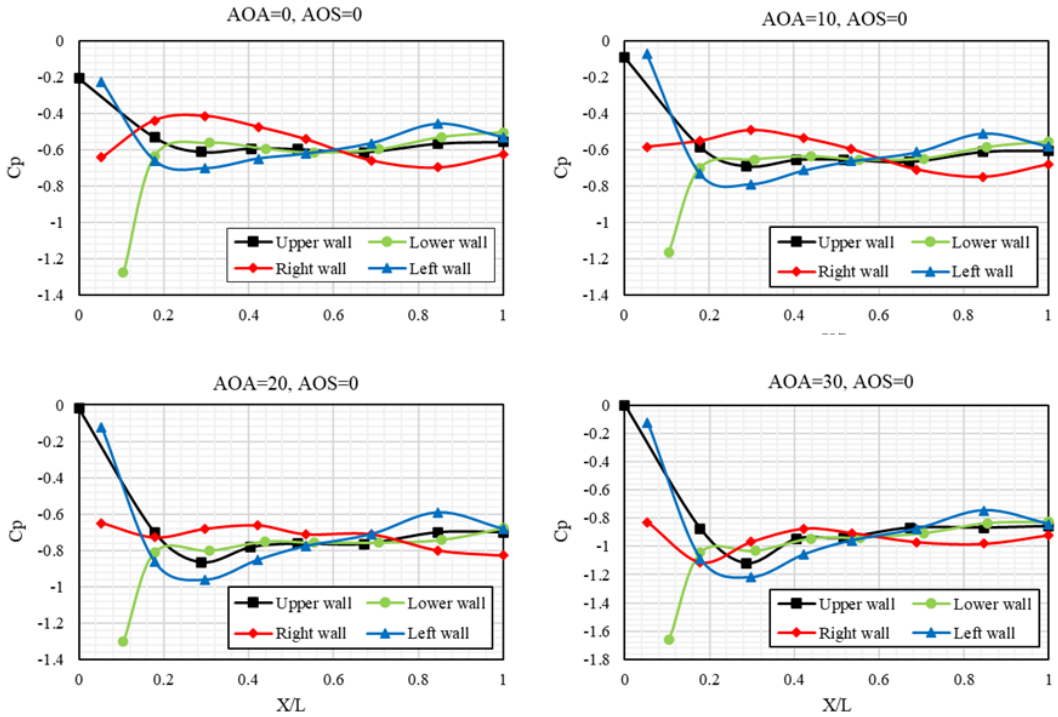


**Fig. 14.** The pressure coefficient is distributed along the duct at different angles of attack and sideslip angles of 0°.

Specifically, it decreases from -0.2 at a zero angle of attack to approximately zero at 30° (Fig. **14**), as increasing the angle of attack leads to an increase in the pressure coefficient in this region.

Naturally, the negative value of the pressure coefficient is due to the protruding lip region of the duct. The subsequent decrease in the pressure coefficient along the curve is attributed to the suction created within the air inlet duct. Considering the flow regime in this phase, owing to the low free stream velocity relative to the engine suction, the flow accelerates upon entering

the duct. Consequently, the pressure coefficient downstream is lower than at the entrance. Given the curvature of the duct's upper wall, small-scale increases and decreases in the pressure coefficient are observed. However, the overall trend is increasing (due to the diffuser-like geometry of the duct).

Bottom Wall: In this region, there is no support from the fuselage; therefore, the flow enters the duct with a high deflection angle due to the angle of attack. Therefore, the flow moves faster over the duct lip, and the pressure coefficient is the lowest in this region. As with the upper wall, because of the minor curvatures of the bottom surface within the duct, small fluctuations in the pressure coefficient are again noticed, and they gradually rise. This behavior can be attributed to the fact that the duct geometry dominates the diffuser effect over the surface curvatures.

Inner (Left) Wall: The flow behavior, in this case, resembles that of the upper duct wall, as the supportive effect of the fuselage is also present, and the flow experiences minimal turning upon entering the duct lip. For this reason, the pressure coefficient at the duct entrance is negative but close to zero.

As the flow enters the duct, the pressure coefficient abruptly decreases due to the suction phenomenon. Because of the higher curvature gradient of the inner duct wall in this case, the pressure coefficient variations are more significant than those on the upper wall. Initially, the surface curves outward, indicating local flow acceleration and a decrease in the pressure coefficient. However, as the surface curves inward downstream, the flow experiences an increase in pressure, leading to an increase in the pressure coefficient.

Outer (Right) Wall: Considering the low free stream velocity at the test facility relative to the suction flow within the duct, the streamlines experience a reduction in area upon entering the duct. Consequently, the flow undergoes a significant deflection at the duct entrance (although less severe than the bottom wall since the duct experiences an angle of attack, which reduces the pressure coefficient at the entrance). The flow behavior within the duct for this region is similar to that of the inner wall, with the exception that the conditions for increasing and decreasing the pressure coefficient are reversed due to the inverted curvature form of the duct.

The following figures present the pressure coefficient distributions within the air inlet duct for various angles of attack. As observed, two fundamental trends characterize the behavior of these plots:

First, as the angle of attack increases, the LEX effect increases, and the pressure coefficient at the flow entrance from the upper wall increases. Secondly, as the angle of attack increases, the average pressure coefficient values within the duct are lower, and the influence of the inner duct wall curvatures on the pressure coefficient changes is less. Third, as a result of the higher angle of attack and the corresponding increase in flow turning over the lower duct lip, a greater reduction in the pressure coefficient is experienced.

### 4.3.2 Analysis of the Effect of Sideslip Angle Variation on the Static Pressure Coefficient Distribution on the Duct Walls

In this section, the variations in the pressure coefficient on the duct's inner walls are investigated under the influence of the sideslip angle.

According to the experimental results for different sideslip angles, no significant differences in the flow behavior within the duct are observed compared to the aforementioned plots. The primary changes are related to the air inlet duct lip (Fig. **15**).

Given the lack of an angle of attack in the flow, there is no significant variation in the pressure coefficient on the upper wall. This is due to the fact that the flow behavior in this region is highly sensitive to the LEX. The pressure coefficient at the inner wall increases only at the angle of -15° of the sideslip. In this condition, the flow impingement angle is greater than zero, and therefore, the pressure coefficient in this region is higher than in the previous case. In the case of the outer wall section, when the sideslip angle is negative, the flow deflection into the duct is higher, which results in a lower pressure and a more negative pressure coefficient. However, as the sideslip angle increases, the curvature of the streamlines passing over the duct lip decreases, which in turn leads to an increase in the pressure coefficient in this region

.

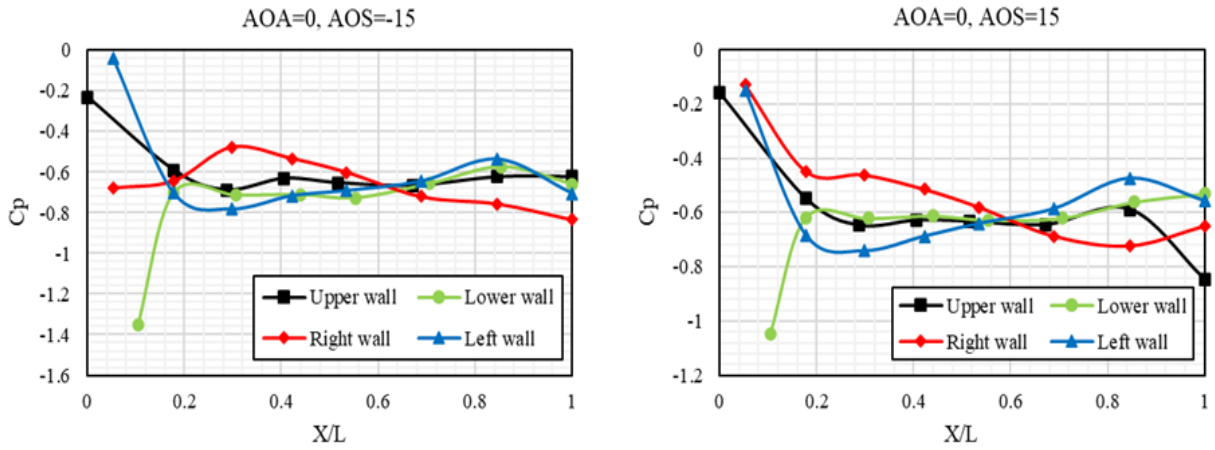


**Fig. 15.** Variation of the pressure coefficient within the duct for different sideslip angles and a zero angle of attack.

The case is a little different for the bottom wall. In order to explain the physics of the flow over the lip in this area, it is pertinent to refer to Fig. **16**. Since the duct inlet geometry has an angle in both the top and side views, the flow is deflected to different extents when it passes over the duct lip surface at different angles of attack. The change of curvature in a particular range over a short distance means that the flow accelerates rapidly, and the pressure coefficient decreases, and conversely. As a result, when the sideslip angle is negative, the duct lip on the bottom wall accelerates significantly, which leads to a reduction in the pressure coefficient in this area. The same situation can be observed on the upper wall (at the sideslip angle) and the inner and outer walls (at the angle of attack).

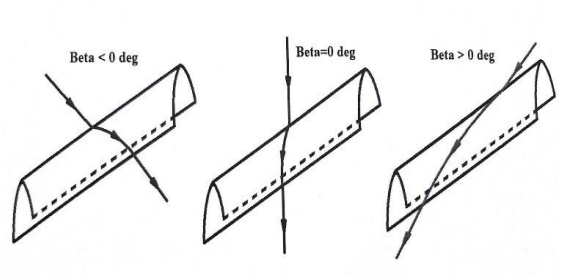


**Fig. 16.** Schematic representation of the flow passage over the upper and lower duct lips at different sideslip angles.

## 5. CONCLUSION

This study analyzed the flow characteristics in a Y-shaped duct integrated with a fuselage containing a LEX. The basic assessment criteria for the duct, namely pressure recovery and flow distortion at the exit plane of the duct, were determined and depicted. Based on the graphs presented in this study, pressure recovery in the channel decreases with an increase in the angle of attack. This happens due to the increase in the flow's reversed pressure gradient and the greater boundary layer growth across the channel. Furthermore, pressure loss within the channel increases with an increase in the sideslip angle due to the entry of the body surface boundary layer into the channel.

With the presence of attack angles and boundary layer growth in some parts of the channel body, flow distortion increases at the channel outlet. In a negative attack angle, the upper part of the channel outlet experiences the flow's lack of uniformity; however, the lower part of the channel outlet experiences the flow's lack of uniformity in a positive attack angle.

Moreover, the results indicate that the presence of a sideslip angle increases the flow distortion at the channel outlet by 5% to 7%. The examined channel has a stagger angle, positively influencing its performance at high attack angles and sideslip. The presence of this angle results in a significant decrease in the intense pressure gradients generated on the channel lip at positive attack angles, demonstrating its effect on the total pressure loss decrease at the channel's end. The current study results reveal that the maximum total pressure loss in the examined channel equals 1.75%, occurring at an attack angle of 40° and a sideslip angle of 15°. Furthermore, the maximum flow distortion parameter at the channel end equals 29.2%, which is provided at a -10° attack angle and a 15° sideslip angle.

## NOMENCLATURE:

| | |
|---|---|
| AOA | Angle of attack |
| LEX | Leading-edge extension |
| AOS | Angle of sideslip |
| DC | Distortion coefficient |
| ΔP | Pressure loss |
| PR | Total pressure recovery |
| L | Duct length |
| $C_P$ | pressure coefficient |

## CONFLICT OF INTEREST

The authors declare that they have no conflict of interest.

## REFERENCE

[1]. J. Seddon and E. L. Goldsmith, *Intake Aerodynamics*, 2nd ed., Oxford, UK: Blackwell Science, 1999.

[2].M. Yadegari, "An optimal design for S-shaped air intake diffusers using simultaneous entropy generation analysis and multi-objective genetic algorithm," *The European Physical Journal Plus*, vol. 136, no. 10, 2021, Art. no. 1019, https://doi.org/10.1140/epjp/s13360-021-01999-4.

[3] M. H. Moghimi EsfandAbadi, A. Mohammadi, M. H. Djavareshkian, "Design and analysis of supersonic inlet for ramjet engines: Aerodynamic considerations and performance optimization,: *Journal of Aerospace Science and Technology*, vol. 17, no. 1, pp. 47-59, 2024, https://doi.org/10.22034/jast.2023.421137.1165.

[4].S. Wellborn, B. Reichert, and T. Okiishi, "An experimental investigation of the flow in a diffusing S-duct," in *28th Joint Propulsion Conference and Exhibit*, Nashville, TN, USA, 1992.

[5]. C. Fiola and R.K. Agarwal, "Simulation of secondary and separated flow in a diffusing S-duct," *Journal of Propulsion and Power*, vol. 31, no. 1, pp. 180-191, 2015, https://doi.org/10.2514/1.B35275.

[6].E. Manca, "Unsteady aerodynamic investigation of the flow within an optimized S-duct intake," MSc Thesis, Cranfield University, Cranfield, 2016.

[7]. S. Ghosh, D. Pratihar, K. Maiti, and P.K. Das, "An evolutionary optimization of diffuser shapes based on CFD simulations," *International Journal for Numerical Methods in Fluids*, vol. 63, no. 10, pp. 1147–1166, 2010, https://doi.org/10.1002/fld.2124.

[8]. A. Rigobello, "A multi-objective shape optimization of an S-duct intake through NSGA-II genetic algorithm," MSc Thesis, University of Padua, Italy, 2016.

[9]. L. Zeng, D. Pan, S. Ye, and X. Shao, "A fast multi objective optimization approach to S-duct scoop inlets design with both inflow and outflow," *Proceedings of the Institution of Mechanical Engineers, Part G: Journal of Aerospace Engineering*, vol. 233, no. 9, pp. 3381–3394, 2018, https://doi.org/10.1177/0954410018795806.

[10]. E. Immonen, "Shape optimization of annular S-ducts by CFD and high-order polynomial response surfaces," *Engng Computations*, vol. 35, no. 2, pp. 932–954, https://doi.org/10.1108/EC-08-2017-0327.

[11]. W. Gan and X. Zhang, "Design optimization of a three-dimensional diffusing S-duct using a modified SST turbulent model," *Aerospace Science and Technology*, vol. 63, pp. 63–72, 2017, https://doi.org/10.1016/j.ast.2016.12.016.

[12]. S. H. Sadatpour and A. Madadi, "Optimization of S-shaped inlet diffuser; improvement of total pressure loss and flow uniformity," *Amirkabir Journal of Mechanical Engineering*, vol. 52, no. 11, pp. 3171-3186, 2021, https://doi.org/10.22060/mej.2019.16078.6265.

[13]. K. R. Yadav, A. Jain and A. Ranjan Paul, "Flow characteristics and separation control in a transitional twin air-intake," *Proceedings of the Institution of Mechanical Engineers, Part G: Journal of Aerospace Engineering*, vol. 237, no. 2, pp. 1–11, 2022, https://doi.org/10.1177/09544100221103652.

[14]. R. K. Singh, S. N. Singh, and V. Seshadri, "Performance and flow characteristics of double-offset Y-shaped aircraft intake ducts," *Journal of Aircraft*, vol. 45, no. 4, pp. 1230–1245, 2008, https://doi.org/10.2514/1.34137.

[15]. J. Nugent, "Non-steady flow of a twin-duct propulsion system and airplane coupling slightly below a Mach number of 2.0," NASA, TM X-54, 1959.

[16]. B. Li and D. W. Wang, "Numerical computation for a bifurcated Y-inlet," *Journal of Nanjing University of Aeronautics & Astronautics*, vol. 36, no. 1, pp. 6-10, 2004.

[17]. N. J. Martin and C. A. Holzhauser, "Analysis of factors influencing the stability characteristics of symmetrical twin intake air-induction system," NACA TN-2049, 1950.

[18]. K. Sudhakar and N. Ananthkrishnan, "Jump phenomena in Y-shaped intake ducts," *Journal of Aircraft*, vol. 33, no. 2, pp. 438–439, 1996, https://doi.org/10.2514/3.46957.

[19]. S. N. Patel, S. N. Singh, and V. Seshadri, "Characteristics of Y-shaped rectangular diffusing duct at different inflow conditions," *Journal of Aircraft*, vol. 42, no. 1, pp. 113–120, 2005, https://doi.org/10.2514/1.4690.

[20]. K. Saha, "Aerodynamic studies on the flow characteristics of intake ducts," Ph.D. dissertation, Indian Institute of Technology Delhi, India, 2007.

[21]. A. R. Paul, S. Joshi, A. Jindal, S. P. Maurya, and A. Jain, "Experimental studies of active and passive flow control techniques applied in a twin air-intake," *Scientific World Journal*, vol. 2013, no. 1. 2013, Art. no. 523759, https://doi.org/10.1155/2013/523759.

[22]. R. K. Singh, S. N. Singh, and V. Seshadri, "Effect of corner rounding on the performance of the double offset Y-shaped aircraft intake duct," *Proceedings of the Institution of Mechanical Engineers, Part G: Journal of Aerospace Engineering*, vol. 222, no. 7, pp. 969-983, 2020, https://doi.org/10.1243/09544100JAERO368

[23]. R. K. Singh, S. N. Singh, and V. Seshadri, "Performance and flow characteristics of double-offset Y-shaped aircraft intake ducts," Journal of Aircraft, vol. 45, no. 4, pp. 1230–1245, 2008, https://doi.org/10.2514/1.34137.

[24]. V. M. K. Knotted and S. Mittal, "Flow in a Y-intake at supersonic speeds," *Journal Propulsion Power*, vol. 32, no. 1, pp. 171–187, https://doi.org/10.2514/1.B35699.

[25]. Y. K. K. Rajnath, A. R. Paul, and A. Jain, "Effects of flow control in the presence of asymmetric inflows in twin air-intakes," *Aircraft Engineering and Aerospace Technology: An International Journal*, vol. 92, no. 3, pp. 460–471, https://doi.org/10.1108/AEAT-06-2019-0116.

[26]. Krishnakumar R Yadav, Anuj Jain, Akshoy Ranjan Paul. "low characteristics and separation control in a transitional twin air intake." *Journal of Aerospace Engineering*, vol. 237, no. 3, 2023. p. 516–526, https://doi.org/10.1177/09544100221103652.

[27]. Paul AR, Ranjan P, Upadhyay RR et al., "Passive flow control in twin air intakes." *Proceedings of WASET International Conference on Mathematical and Computational Methods in Science and Engineering (ICMCMSE 2011)*, Paris, France, 24–26 June, Yr. 7,. Vol. 77, no. 56, 2011, pp. 297–304.

[28]. Gabaliya, M. K. and Chaudhary, K., "CFD analysis of performance characteristics of Y-shaped diffuser with combined horizontal and vertical offsets," *Aerospace Science and Technology*, vol. 14, no. 5, 2010, p. 338-347, https://doi.org/10.1016/j.ast.2010.02.008

[29]. M.Yadegari, and A.B. Khoshnevis, "Entropy generation analysis of turbulent boundary layer flow in different curved diffusers in air-conditioning systems." *The European Physical Journal Plus*, vol. 135, no. 6, 2020 p. 534, https://doi.org/10.1140/epjp/s13360-020-00545-y.

[30]. M. Yadegari, and A. Bak Khoshnevis, "A numerical study over the effect of curvature and adverse pressure gradient on the development of flow inside gas transmission pipelines." *Journal of the Brazilian Society of Mechanical Sciences and Engineering*, vol. 42, 2020, pp. 1-15, https://doi.org/10.1007/s40430-020-02495-z

[31]. H. Haghighatjoo, M. Yadegari, and A. Bak Khoshnevis, "Optimization of single-obstacle location and distance between square obstacles in a curved channel." *The European Physical Journal Plus*, 2022. vol. 137, no. 9, 2020, Articl number, 1042, https://doi.org/10.1140/epjp/s13360-022-03260-y.

[32]. M. Yadegari, and A. Bak Khoshnevis, "Investigation of entropy generation, efficiency, static and ideal pressure recovery coefficient in curved annular diffusers." *The European Physical Journal Plus*, vol. 136: 2020, pp. 1-19, https://doi.org/10.1140/epjp/s13360-021-01071-1.

[33]. M. Yadegari, and A.B. Khoshnevis, "Numerical study of the effects of adverse pressure gradient parameter, turning angle, and curvature ratio on turbulent flow in 3D turning curved rectangular diffusers using entropy generation analysis." *The European Physical Journal Plus*, vol. 135, no. 7, 2020, p. 548, https://doi.org/10.1140/epjp/s13360-020-00561-y

**COPYRIGHTS**

Authors retain the copyright and full publishing rights.
Published by Iranian Aerospace Society. This article is an open access article licensed under the Creative Commons Attribution 4.0 International (CC BY 4.0).

**HOW TO CITE THIS ARTICLE**

A. Fazli, A. Abdi, and M. Mahmoodi, "Experimental Study on the Performance of a Symmetrical Twin Air Intake System," *Journal of Aerospace Science and Technology*, Vol. 18, Issue 1, 2025, pp. 58-69.

DOI: https://doi.org/10.22034/jast.2025.462215.1192.

URL: https://jast.ias.ir/article_218670.html